COMPUTATIONAL AEROACOUSTIC PREDICTION OF TRANSONIC ROTOR NOISE BASED ON REYNOLDS-AVERAGED NAVIER-STOKES FLOW SIMULATION

Song Wen-ping *, Han Zhong-hua*, Qiao Zhi-de*
*** National Key Laboratory of Aerodynamic Design and Research, School of Aeronautics, Northwestern Polytechnical University, Xi'an 710072, P.R.China**

Keywords: ***Computational Aeroacoustics, helicopter rotors , Navier-Stokes equations , aeroacoustic noise, Ffowcs Williams-Hawking equation***

Abstract

An efficient and accurate method for predicting the aeroacoustic noise generated by transonic helicopter rotors is investigated. The near-field noise is calculated by numerically solving Reynolds-Averaged Navier-Stokes (RANS) equations using chimera grid methodology. The far-field noise is predicted by using the method based on Ffowcs Williams-Hawkings equation with penetrable data surface (FW-H_{pds}) covering the nonlinear flow region. The computed results are compared with experimental data and good agreement has been achieved. The results are also compared with that of the method based on inviscid flow simulation using Euler equations. It shows that the present method is more accurate for the prediction of High-Speed Impulsive (HSI) noise generated by transonic helicopter rotors.

1 Introduction

Over the past decade, the hybrid method, coupling CFD (Computational Fluid Dynamics) techniques with advanced analytic methods based on acoustic analogy (such as FW-H_{pds} method), has been successfully applied to predict the complicated acoustic field of helicopter rotors.

The Ffowcs Williams-Hawkings （FW-H）equation [1], a rearrangement of Navier-Stokes equations by utilizing general-function theory, provides an accurate theoretical model for describing the propagation of noise from a moving surface to far field. The Farassat1A method of solving the linear part of FW-H equation was developed by Farassat [2] and has been successfully applied in linear-noise prediction [2] for more than 20 years. Farassat1A method predicts discrete-frequency noise quite well, but it would run into complication when predicting nonlinear quadrupole noise of helicopter rotors as the data surface is the blade itself and nonlinear effects are not included in the surface integral. To calculate the nonlinear noise, e.g. High-Speed Impulsive (HSI) noise, Farassat and Mayers [3] derived the general form of Kirchhoff equation and its solution (known as Kirchhoff formulation) to describe the noise radiation from a moving surface. The data surface of Kirchhoff formulation is fictitious and penetrable. The main benefit of Kirchhoff method is in that the nonlinear effect is accounted for by performing the integral on the data surface which covering the nonlinear flow region. Kirchhoff method coupled with the near-field CFD solution (called CFD/Kirchhoff method) has been proved to be accurate and efficient when predicting impulsive noise. More recently, a new form of FW-H equation with a penetrable surface (called FW-H_{pds} equation) was proposed by Crighton etc. [4] to improve the efficiency of solving the quadrupole noise. A new method combining Euler equation simulation with FW-H_{pds} equation was proposed by di Francescantonio [5] and successfully applied in the noise perdition of transonic helicopter rotors in hover. Brentner and Farassat [6] conducted an analytical comparison of FW-H_{pds} method with Kirchhoff method and concluded that FW-H_{pds} method is more

accurate and robust than Kirchhoff method when the data surface is located in the nonlinear flow region. FW-H_{pds} method rapidly shows promises in the study work of a few researchers [6,7] when it is used for predicting the noise generated by helicopter rotors in hover and forward flight. More recently, Farassat emphasized the role of analytical methods in Computational Aeroacoustics and recommended FW-H_{pds} as a very promising method for noise prediction of complicated flow field.

However, according to the experience of the present authors, the accuracy of FW-H_{pds} method is strongly affected by the accuracy of the aerodynamic input data obtained from CFD calculation. To predict non-linear noise generated by transonic rotors, three-dimensional Euler equations were commonly used to consider the nonlinear effect related to shock wave. To consider the influence of viscous effect in near field and get more accurate information of noise sources, this paper uses Reynolds-Averaged Navier-Stokes (RANS) equations to model the nonlinear viscous flow field near the rotor blades. The far-field noise is calculated by a retarded-time integral formula solving FW-H_{pds} equation, with the solution of RANS equations taken as input data.

This paper focused on the accurate and efficient prediction of High-Speed Impulsive (HSI) noise generated by helicopter rotors, illustrated by examples of helicopter rotor in hover; moreover, the presented method is readily applicable to Blade-vortex Interaction (BVI) noise of helicopter rotor if RANS equations are solved by high-order, low-dissipation and low-dispersion scheme.

2 RANS Method for Transonic Helicopter Rotor in Hover

Simulation of quasi-steady flow over helicopter rotors in hover uses a relative coordinate system fixed on rotor blade (see Fig.1). The grids around a single blade are generated, and the flow field only around a single rotor blade is simulated. The influence of other blades is accounted for by performing a periodic boundary condition. Chimera grid methodology is used to effectively capture the viscous effect near rotor blade and implement the periodic boundary condition.

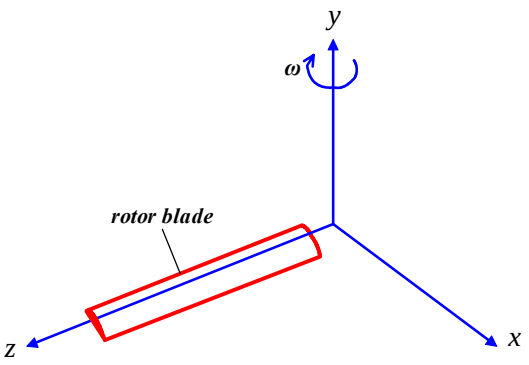

Fig. 1 Schematics of blade-fixed coordinate system

2.1 Chimera Grid Methodology

Using algebraic method based on transfinite interpolation [8] and elliptical smoothing technique, a C-H type rotor grid and a curved H-H type background grid (see Fig.2) are generated. The blade grid is for the simulation of viscous flow around the rotor blades and the captures of the near-field wake; the background grid is for the capture of far-field wake and for the convenient treatment of periodic boundary condition. The flow information between rotor grid and background grid is exchanged by chimera grid techniques (see Ref. [9]). The grid system and the grid near the rotor blade are illustrated in Fig.2 and Fig.3, respectively.

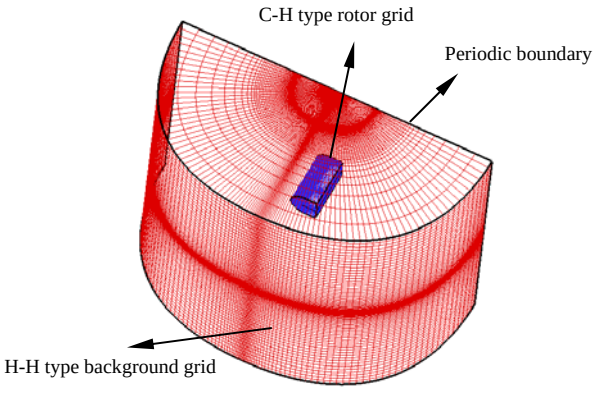

Fig.2 Schematics of chimera grid for a single rotor blade

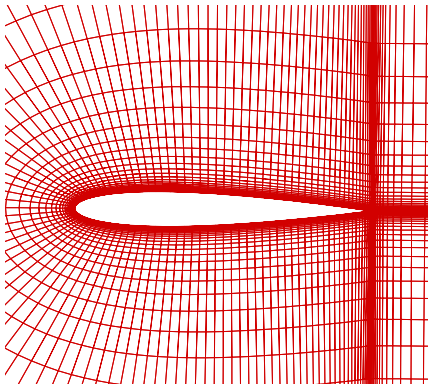

Fig.3 Schematics of one section of rotor grid

2.2 Governing Equations and Solution

Three-dimensional unsteady RANS equations in a relative coordinate system fixed on rotor blade can be written as

$$\iiint_V \frac{\partial \boldsymbol{W}}{\partial t} dV + \iint_S (\overline{\overline{\boldsymbol{F}}} - \overline{\overline{\boldsymbol{F}}}_v) \otimes \boldsymbol{n} dS + \iiint_V \boldsymbol{G} dV = 0 \quad (1)$$

where, V is the control volume, $S, \boldsymbol{n}$ denote boundary of control volume and its unit-normal-outer vector, respectively. The flow variable vector, inviscid flux vector, viscous flux vector and source terms are

$$\boldsymbol{W} = \begin{bmatrix} \rho \\ \rho u \\ \rho v \\ \rho w \\ \rho E \end{bmatrix}, \overline{\overline{\boldsymbol{F}}} = \begin{bmatrix} \rho(\boldsymbol{q}-\boldsymbol{q}_b) \\ \rho u(\boldsymbol{q}-\boldsymbol{q}_b) + p\boldsymbol{i}_x \\ \rho v(\boldsymbol{q}-\boldsymbol{q}_b) + p\boldsymbol{i}_y \\ \rho w(\boldsymbol{q}-\boldsymbol{q}_b) + p\boldsymbol{i}_z \\ \rho E(\boldsymbol{q}-\boldsymbol{q}_b) + p\boldsymbol{q} \end{bmatrix},$$
$$\overline{\overline{\boldsymbol{F}}}_v = \begin{bmatrix} 0 \\ \tau_{xx}\boldsymbol{i}_x + \tau_{xy}\boldsymbol{i}_y + \tau_{xz}\boldsymbol{i}_z \\ \tau_{xy}\boldsymbol{i}_x + \tau_{yy}\boldsymbol{i}_y + \tau_{zy}\boldsymbol{i}_z \\ \tau_{xz}\boldsymbol{i}_x + \tau_{yz}\boldsymbol{i}_y + \tau_{zz}\boldsymbol{i}_z \\ f_5\boldsymbol{i}_x + g_5\boldsymbol{i}_y + h_5\boldsymbol{i}_z \end{bmatrix}, \boldsymbol{G} = \begin{bmatrix} 0 \\ \rho\omega w \\ 0 \\ -\rho\omega u \\ 0 \end{bmatrix} \quad (2)$$

where, ρ, u, v, w, E represent density, components of velocity vector, total energy per unit mass, respectively; ω is angular velocity of rotor blade; $\boldsymbol{i}_x, \boldsymbol{i}_y, \boldsymbol{i}_z$ denote the unit vector in the blade-fixed coordinate system; $\boldsymbol{q} = u\boldsymbol{i}_x + v\boldsymbol{i}_y + w\boldsymbol{i}_z$ is the velocity vector; $\boldsymbol{q}_b = \boldsymbol{\omega} \times \boldsymbol{r}$ denote the velocity of the boundary of the control volume. Pressure and temperature are given by the equation of state

$$\begin{aligned} p &= \rho(\gamma - 1)[E - 0.5(u^2 + v^2)] \\ T &= p / \rho \end{aligned} \quad (3)$$

The additional variables in Eq. (2) are:

$$\begin{aligned} f_5 &= u\tau_{xx} + v\tau_{xy} + w\tau_{xz} + k\frac{\partial T}{\partial x} \\ g_5 &= u\tau_{xy} + v\tau_{yy} + w\tau_{yz} + k\frac{\partial T}{\partial y} \\ h_5 &= u\tau_{xz} + v\tau_{yz} + w\tau_{zz} + k\frac{\partial T}{\partial z} \\ \tau_{xx} &= 2\mu u_x + \lambda(u_x + v_y + w_z) \\ \tau_{yy} &= 2\mu v_y + \lambda(u_x + v_y + w_z) \\ \tau_{zz} &= 2\mu w_z + \lambda(u_x + v_y + w_z) \\ \tau_{xy} &= \tau_{yx} = \mu(u_y + v_x) \\ \tau_{yz} &= \tau_{zy} = \mu(v_z + w_y) \\ \tau_{xz} &= \tau_{zx} = \mu(u_z + w_x) \end{aligned} \quad (4)\backslash$$

where, k is the coefficient of thermal conductivity and is determined by using the assumption of constant Prandtl number. The bulk viscosity λ is taken to be $-2/3\mu$ according to Stokes's hypothesis. For turbulent flow, the total viscosity μ is calculated as

$$\mu = \mu_l + u_t \quad (5)$$

where, μ_l is molecular viscosity calculated by Sutherland law, and eddy viscosity μ_t is determined by turbulence model. Then, Eq.(1) are called Reynolds-averaged Navier-Stokes equations(RANS). In present work, Baldwin-Lomax algebraic turbulence model is used for all the calculation.

The governing equations are solved by a Finite-Volume Method developed by Jameson. The details can be found in Ref. [10] and Ref. [11].

3 Acoustic Method Based on FW-H_{pds} Equation

3.1 FW-H_{pds} Equation

FW-H equation has been taken as the most general form of the Lighthill acoustic analogy.

In 1969, Ffowcs Williams and Hawkings [1] rearranged the Navier-Stokes equation in fluid dynamic by applying general functions theory, and obtained an inhomogeneous wave equation (namely the well-known FW-H equations) which can give the exact governing equation of acoustic field generated by a wall boundary in arbitrary motion. Consider a piece-wise smooth surface defined by $f(\boldsymbol{x}_i, t) = 0$, which surrounding rotor blade or other types of wall

boundary moving in a stationary fluid., Assuming that $\nabla f = \boldsymbol{n}_i$ and $\partial f/\partial t = -v_n$ ($\boldsymbol{n}_i$ is the unit normal outer vector and $\boldsymbol{v}$ is the velocity vector of control surface), then the FW-H equation can be written as

$$\begin{aligned}(\frac{1}{c^2}\frac{\partial^2}{\partial t^2}-\frac{\partial^2}{\partial \boldsymbol{x}_i^2})p'(\boldsymbol{x}_i,t) &= \frac{\bar{\partial}}{\partial t}\{[(\rho_0 v_n+\rho(u_n-v_n)]\delta(f)\} \\ &-\frac{\bar{\partial}}{\partial \boldsymbol{x}_i}\{[-\boldsymbol{P}'_{ij}\cdot\boldsymbol{n}_j+\rho\boldsymbol{u}_i(u_n-v_n)]\delta(f)\} \\ &+\frac{\bar{\partial}^2}{\partial \boldsymbol{x}_i\boldsymbol{x}_j}[\boldsymbol{T}_{ij}H(f)]\end{aligned} \quad (6)$$

Where, $c,\rho,\boldsymbol{u}_i,\boldsymbol{P}_{ij}$ denotes speed of sound, density, tensors of velocity and stress, respectively; p' is acoustic pressure; $\boldsymbol{T}_{ij}=-\boldsymbol{P}'_{ij}+\rho\boldsymbol{u}_i\boldsymbol{u}_j-c^2\rho'\boldsymbol{\delta}_{ij}$ is Lighthill stress tensor and $\boldsymbol{\delta}_{ij}$ is Kronecker delta ; Subscript " $_0$ " indicates the free-stream undisturbed quantities, and superscript "′" denotes the disturbed values; $H(f)$ is Heaviside function and $\delta(f)$ is Dirac function which satisfy $H(f)=\begin{cases}1 & f(\boldsymbol{x}_i,t)>0\\ 0 & f(\boldsymbol{x}_i,t)<0\end{cases}$ and $\delta(f)=\dfrac{\bar{\partial}H(f)}{\partial f}$.

Note that the control surface $f(\boldsymbol{x}_i,t)=0$ in equation (6) can be taken as a fictitious surface that allows the flow pass through [4]. Then equation is just the so-called FW-H equation with "penetrable data surface"(FW-H_{pds} equation).

Provided that the moving surface $f(\boldsymbol{x}_i,t)=0$ is coincident with the rotor-blade surface, the solid boundary condition $u_n=v_n$ can be applied to equation (6), which yields the common-used form of FW-H equation:

$$(\frac{1}{c^2}\frac{\partial^2}{\partial t^2}-\frac{\partial^2}{\partial \boldsymbol{x}_i^2})p'(\boldsymbol{x},t)=\frac{\bar{\partial}}{\partial t}[(\rho_0 v_n)\delta(f)]-\frac{\bar{\partial}}{\partial \boldsymbol{x}_i}[l_i\delta(f)]+\frac{\bar{\partial}^2}{\partial \boldsymbol{x}_i\boldsymbol{x}_j}[\boldsymbol{T}_{ij}H(f)] \quad (7)$$

where, $\boldsymbol{l}_i=-\boldsymbol{P}'_{ij}\cdot\boldsymbol{n}_j$. The three source terms of the right-hand side of the Equation (7) are known as monopole (or thickness), dipole (or loading) and quadrupole source terms, respectively. Farassat derived the solutions of thickness and loading noise in equation (7), and these solutions are well known as Farassat 1A formula [2].

3.2 The Solution of FW-H_{pds} Equation

Note that FW-H equation (7) is essentially a special form of FW-H_{pds} equation when $u_n=v_n$. Referring Brentner and Farassat's derivation [6], the solution of FW-H_{pds} equation can be written out according to Farassat 1A formula. Actually, assuming that

$$\begin{aligned}\boldsymbol{U}_i &= (1-\frac{\rho}{\rho_0})\boldsymbol{v}_i+\frac{\rho\boldsymbol{u}_i}{\rho_0} \\ \boldsymbol{L}_i &= -\boldsymbol{P}'_{ij}\cdot\boldsymbol{n}_j+\rho\boldsymbol{u}_i(u_n-v_n)\end{aligned} \quad (8)$$

Then the FW-H_{pds} equation becomes

$$(\frac{\partial^2}{c^2\partial t^2}-\frac{\partial^2}{\partial \boldsymbol{x}_i^2})p'(\boldsymbol{x},t)=\frac{\bar{\partial}}{\partial t}[\rho_0 U_n\delta(f)]-\frac{\bar{\partial}}{\partial \boldsymbol{x}_i}[\boldsymbol{L}_i\delta(f)]+\frac{\bar{\partial}^2}{\partial \boldsymbol{x}_i\boldsymbol{x}_j}[\boldsymbol{T}_{ij}H(f)] \quad (9)$$

The above form is very similar to equation (7). Its solution can be written as

$$p'(\boldsymbol{x}_i,t)=p'_S(\boldsymbol{x}_i,t)+p'_V(\boldsymbol{x}_i,t) \quad (10)$$

where, the subscript "S" and "V" represent surface integral and volume integral, respectively. When the data surface $f(\boldsymbol{x}_i,t)=0$ is sufficiently far away from wall boundary and covering most of the acoustic noise source, $p'_V(\boldsymbol{x}_i,t)$ can be reasonably neglected. And one can immediately write out the detail form of $p'_S(\boldsymbol{x}_i,t)$ according to Farassat 1A formula presented in Ref. [2]. It takes the form

$$p'_S(\boldsymbol{x}_i,t)=p'_M(\boldsymbol{x}_i,t)+p'_L(\boldsymbol{x}_i,t) \quad (11)$$

And

$$\begin{aligned}p'_M(\boldsymbol{x}_i,t) &= \frac{1}{4\pi}\int_{f=0}\left[\frac{\rho_0 c_0(\dot{M}_n+\dot{n}_M)}{r(1-M_r)^2}\right]_{ret}dS \\ &+\frac{1}{4\pi}\int_{f=0}\left[\frac{\rho_0 c_0 M_n\dot{M}_r}{r(1-M_r)^3}\right]_{ret}dS \\ &+\frac{1}{4\pi}\int_{f=0}\left[\frac{\rho_0 c_0^2 M_n(M_r-M^2)}{r^2(1-M_r)^3}\right]_{ret}dS\end{aligned}$$

$$\begin{aligned}p'_L(\boldsymbol{x}_i,t) &= \frac{1}{4\pi}\int_{f=0}\left[\frac{\dot{L}_r}{c_0 r(1-M_r)^2}\right]_{ret}dS \\ &+\frac{1}{4\pi}\int_{f=0}\left[\frac{L_r-L_M}{r^2(1-M_r)^2}\right]_{ret}dS \\ &+\frac{1}{4\pi}\int_{f=0}\left[\frac{L_r\dot{M}_r}{c_0 r(1-M_r)^3}\right]_{ret}dS \\ &+\frac{1}{4\pi}\int_{f=0}\left[\frac{L_r(M_r-M^2)}{r^2(1-M_r)^3}\right]_{ret}dS\end{aligned}$$

where, the subscript "ret" represent retarded time, and

$$\boldsymbol{M}_i = \boldsymbol{U}_i / c_0, M_r = \boldsymbol{M}_i \cdot \boldsymbol{r}_i / r \quad M_n = \boldsymbol{M}_i \cdot \boldsymbol{n}_i$$
$$\dot{M}_n = \dot{\boldsymbol{M}}_i \cdot \boldsymbol{n}_i, \dot{M}_r = \dot{\boldsymbol{M}}_i \cdot \boldsymbol{r}_i / r, \dot{n}_M = \dot{\boldsymbol{n}}_i \cdot \boldsymbol{M}_i$$
$$L_r = \boldsymbol{L}_i \cdot \boldsymbol{r}_i / r, L_M = \boldsymbol{L}_i \cdot \boldsymbol{M}_i, \dot{L}_r = \dot{\boldsymbol{L}}_i \cdot \boldsymbol{r}_i / r$$

If $f(\boldsymbol{x}_i, t) = 0$ is selected as the blade surface, $p'_S(\boldsymbol{x}_i, t)$ will recover to Farassat 1A formula. And if $f(\boldsymbol{x}_i, t) = 0$ is fictitious, penetrable surface in 3-D space, $p'_S(\boldsymbol{x}_i, t)$ no longer has the physical meaning of thickness and dipole noise.

The main advantage of FW-H_{pds} method is in that the nonlinear effect can be accounted for by performing the surface integral (denoted by $p'_S(\boldsymbol{x}_i, t)$) on the data surface covering the nonlinear flow region. In other words, the contribution of nonlinear noise source inside the data surface can be calculated by surface integral and the complicated volume integral can be avoided reasonably.

When one takes insight into formula (11), one can find out that only the flow variables ρ, u, v, w, p on data surface $f(\boldsymbol{x}_i, t) = 0$ are need as input data. Once these variables are specified, the acoustic pressure of a given observing point in far field can be calculated by a numerical integral on data surface. Coupled with modern CFD techniques, FW-H_{pds} method is proved to be very effective and relatively accurate for predicting transonic rotor noise (such as HSI noise).

3.3 Choices of Data Surface and Solution of Retarded-Time Equation

In order to perform the integral in formula (11), two key points should be highlighted in this paper. They are: 1) choices of data surface, 2) solution of retarded-time equation.

To perform the integration of time-domain integral method (Such as Formula 11), the first key point is the appropriate choices of data surface. There are two types of data surfaces that are generally used in rotor noise prediction, namely rotating data surface and non-rotating data surface, and both are used in this study. The rotating surface is selected as some surfaces of CFD grid that have the same angular velocity of the rotors. The main advantage of using rotating surface is in that the aerodynamic data on the data surface can be directly obtained from CFD solutions; hence the numerical interpolation is avoided. The non-rotating data surface is defined as a cylindrical surface that is relatively stationary with respect to blade hub. The advantage of non-rotating surface is that with it the retarded-time can be solved explicitly, as will be shown in the following formula (12). The non-rotating surface is divided into elements along its axial and circular direction. To quickly obtain the aerodynamic data of these elements, a 3-D linear interpolation is preformed from CFD solution. A fast searching methodology based inverse map is used to improved the efficiency of searching the contribution CFD grid cell for a considering point.

Another key point is the solution of retarded-time equation. For the noise prediction of helicopter rotors in hover, the retarded-time equation can be written as

$$\tau = t - \frac{1}{c_0}\left| \boldsymbol{x}_0 - \begin{bmatrix} \cos(\omega_s \tau) & 0 & -\sin(\omega_s \tau) \\ 0 & 1 & 0 \\ \sin(\omega_s \tau) & 0 & \cos(\omega_s \tau) \end{bmatrix} \boldsymbol{y}_0 \right| \qquad (12)$$

where τ is the retarded time for a given observing point; $\boldsymbol{x}_0$, $\boldsymbol{y}_0$ denotes the coordinate vectors of the observing and the source point at zero time, respectively. ω_s is the angular velocity of rotating data surface, which is chosen the same value as the angular velocity of rotors. Note that $\omega_s = 0$ corresponds to the non-rotating data surface. For $\omega_s = 0$, Eq. (12) is an explicit formula for τ. However, the solution of this equation cannot be explicitly deduced if $\omega_s \neq 0$. In this paper, a solution method base on simple iteration technique is developed for rotating data surface and a good convergence is achieved.

4 Results and Discussing

All simulations in this section are performed using $169 \times 49 \times 65$ C-H type rotor grid and $101 \times 81 \times 91$ H-H type background grid (as illustrated in Fig.2 and Fig.3). The rotor grids have the first near-surface grid point below y+ = 0.7 to ensure the sublayer of the turbulent shear flow is sufficiently resolved. The definition of

Reynolds number is based on the chord and the tip Mach number of rotor blade.

4.1 Validation of RANS flow solver

For noise perdition using CFD combined with FW-H_{pds} Method, the accuracy of near-field CFD solution has significant effect on the predicting accuracy of far-field noise. Therefore, it is necessary to check the accuracy of the RANS flow solver before performing noise prediction.

The simulation of flow over Caradonna rotor [12] is performed to validate the RANS flow solver. The experiment of Caradonna provided a set of data for benchmarking the numerical simulation of helicopter rotor in hover. The rotor model for Caradonna's experiment employed two-bladed rotor with an NACA 0012 profile. The blades were untwisted and untapered. An aspect ratio of 6.0 was used, and the rotor diameter was set at 2.288 m.

The first validation is the subsonic none-lifting case with the tip Mach number of 0.52 and a Reynolds number of 2.33×10^6. Fig.4 (a) and Fig4 (b) show the comparison of computed pressure distribution and experimental data for two different locations (r/R=0.68 and r/R=0.89) along the rotor span, indicating that the computational results are in excellent agreement with experimental data.

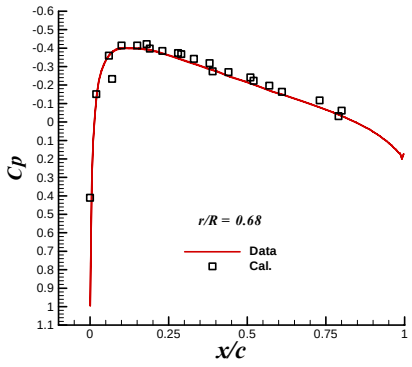

(a) r/R=0.68

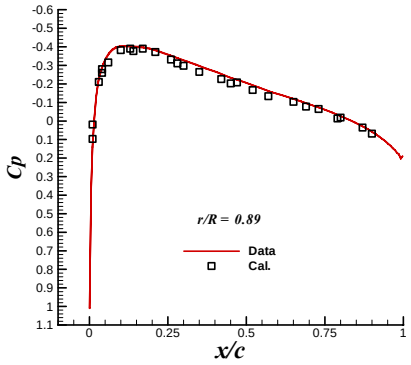

(b) r/R=0.89

Fig.4 Comparison of computed pressure distribution and experimental data ($Ma_{tip} = 0.52, \theta_c = 0^0, \mathrm{Re} = 2.33\times10^6$).

The second validation is the transonic lifting case with the tip Mach number of 0.877, a Reynolds number of 3.93×10^6 and a collective pitch angle of 8^0. The comparison of computed pressure distribution and experimental data for two different locations (r/R=0.89 and r/R=0.96) is demonstrated in Fig.5 (a) and Fig5 (b), and the agreement is very well. It is also shown that the shock wave occurs in the flow field near the blade tip is correctly captured.

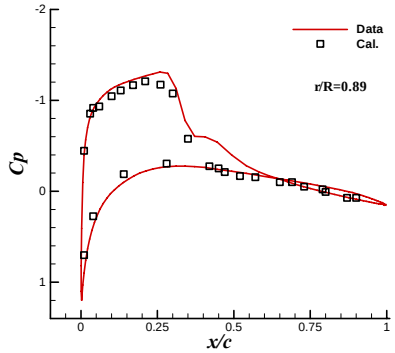

(a) r/R=0.89

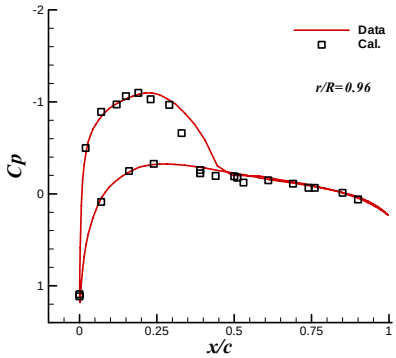

(b) r/R=0.96

Fig.5 Comparison of computed pressure distribution and experimental data ($Ma_{tip} = 0.877, \theta_c = 8^0, \mathrm{Re} = 3.93\times10^6$).

4.2 Validation of RANS/FW-H_{pds} Method

To validate present RANS/FW-H_{pds} Method for HSI noise of transonic rotors, an UH-1H model is adopted. UH-1H rotor is a one-seventh scale two-bladed model with untwisted rectangular-platform blades and NACA0012 airfoil section. The rotor blade has an aspect ratio of 13.71 and a chord length of 0.0762m. The observing microphone is located 3.09R away from the rotative axis(R is the radius of rotor. see Fig.6). The experimental data was published by Boxwell etc. in Ref.[11].

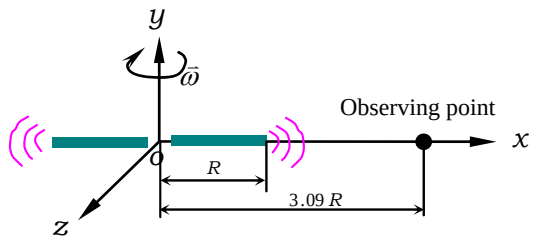

Figure 6 observing location for UH-1H rotor in hover

The near field of UH-1H rotor is simulated by RANS method presented in section 2. The rotating data surface consists some of the grid surfaces of C-H type rotor grid (see Fig.7) and the flow variables on the data surface are calculated directly from RANS solution on rotor grid; non-rotational data surface is constructed as a circular cylinder (see Fig.8). The cylinder is divided as 1440×30 surface elements (1440 segments along the circular direction and 30 segments along the axial direction). The value of flow variables on cylinder is obtained by a 3-D linear interpolation from flow field on background grid.

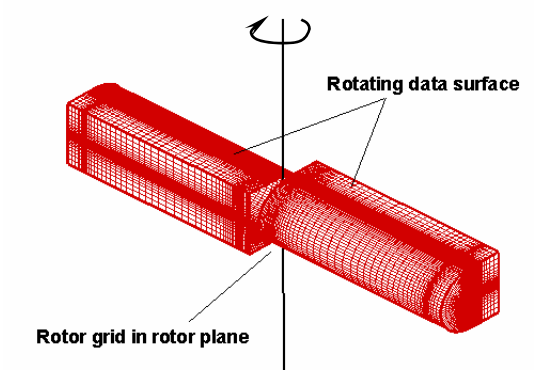

Fig.7 Schematics of rotating data surface

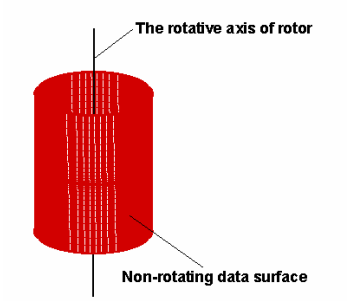

Fig.8 Schematics of non-rotating data surface

Fig.9 and Fig.10 show the comparison of predicted acoustic pressure and experiment data at tip Mach number of 0.85 and 0.95, repectively. Non-rotating circular cylinder with a radius of 1.2R is used as the data surface. The observing point is the same as illustrated in Fig.6.The computed results show good agreement with experimental data. Fig. 11 and Fig 12 show the comparison of predicted acoustic pressure in one period using rotating and non-rotating data surface, and only little difference has been found both for tip Mach number of 0.85 and 0.95. One can conclude that, by RANS/FW-H_{pds} method, both rotating and non-rotating data surface are nearly identically adequate for predicting the nonlinear noise of transonic rotors. The average time for predicting single observing point is about one minute on Pentium IV 3.4G personal computer, which indicates that the present method is very efficient.

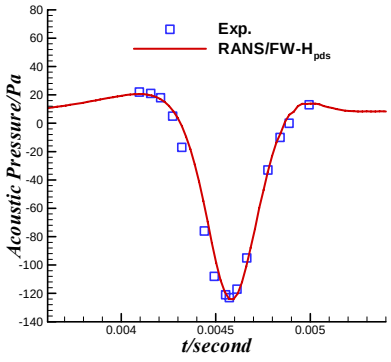

Fig.9 Comparison of predicted acoustic pressure and experimental data ($Ma_{tip} = 0.85$)

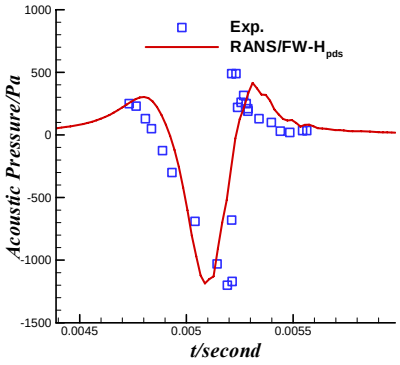

Fig.10 Comparison of predicted acoustic pressure and experimental data ($Ma_{tip} = 0.95$)

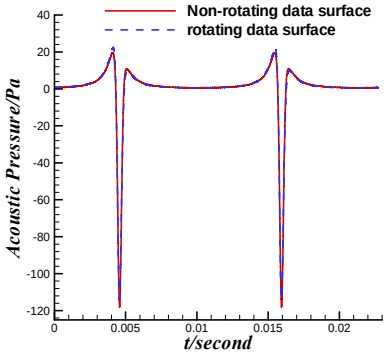

Fig.11 Comparison of predicted acoustic pressure in one period using rotating and non-rotating data surface ($Ma_{tip} = 0.85$)

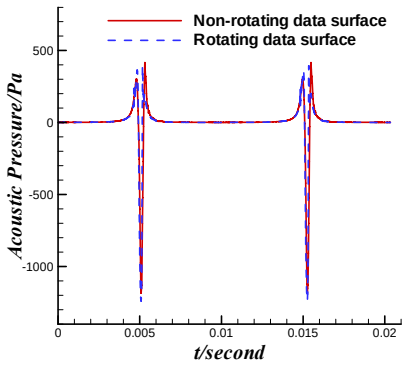

Fig.12 Comparison of predicted acoustic pressure in one period using rotating and non-rotating data surface ($Ma_{tip} = 0.95$)

4.3 Comparison of Different Acoustic Methods

The present RANS/FW-H$_{pds}$ method is compared with Euler/FW-H$_{pds}$ Method and Farassat 1A method. Prediction of HSI noise of UH-1H rotor described in subsection 4.2 is performed. The experimental data can be found in Ref.[13] and Ref.[14]

Fig.13 shows the predicted acoustic pressure versus time for tip Mach number of 0.90 and Reynolds number of 1.6×10^6 。The observing point is located at in-rotor-plane point that is 3.09R away from rotating axis.

Fig.14 shows the predicted acoustic pressure versus time for tip Mach number of 0.88 and Reynolds number of 1.56×10^6 。The observing point is located at in-rotor-plane point that is 1.78R away from rotating axis.

In Fig.13 and Fig.14, the result of Farassat 1A method is linear noise including thickness and loading noise. Compared with Farassat 1A method, RANS/FW-H$_{pds}$ method and Euler/FW-H$_{pds}$ method can predict nonlinear noise, which is clearly demonstrated in Fig.13 and Fig.14. The negative-acoustic-pressure peak calculated by using RANS/FW-H$_{pds}$ is higher and more consistent with the experimental data compared with that calculated by Euler/FW-H$_{pds}$ method. The reason can be explained as that the none-linear noise due to viscous effect and downwash of wake system is taken into account more accurately only when using Navier-Stokes equations.

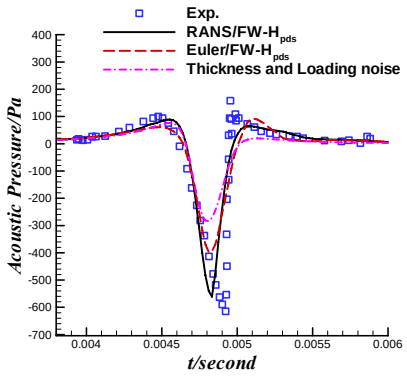

Fig.13 Comparison of predicted acoustic pressure of using different acoustic methods ($Ma_{tip} = 0.90$)

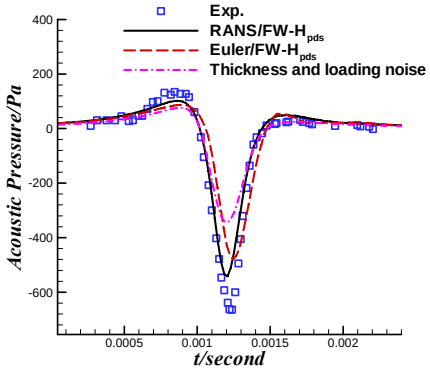

Fig.14 Comparison of predicted acoustic pressure of using different acoustic methods ($Ma_{tip} = 0.88$)

5 Conclusions

A computational aeroacoustic method combining the RANS simulation with FW-H_{pds} method is presented and studied. The results of RANS simulation using Chimera grid methodology is validated adopting Caradonna rotor model. The computed acoustic pressure using presented RANS/FW-H_{pds} for UH-1H rotor is compared with experimental data and show good agreement at different tip Mach numbers. The comparison between RANS/FW-H_{pds} method and Euler/FW-H_{pds} method is made and show that RANS/FW-H_{pds} method is more accurate due to the capture of viscous effect and wake systems in the flow over rotor blades.

The presented methods are readily applicable to Blade-vortex Interaction (BVI) noise of helicopter rotor if RANS equations are solved by high-order, low-dissipation and low-dispersion scheme.

References

[1] Ffowcs Williams J E, Hawkings D L. Sound Generated by Turbulence and Surfaces in Arbitrary Motion [J]. Philosophical Transactions of the Royal Society, 1969, A264(1151): 321～342.

[2] Farassat F. Linear Acoustic Formulas for Calculation of Rotating Blade Noise[R]. AIAA Paper 83-0688, 1983.

[3] Farassat F, Myers M K. Extension of Kirchhoff's Formulation to Radiation from Moving Surface [J]. Journal of Sound and Vibration, 1988, 123(3):451～460.

[4] Crighton, D.G., Dowling, A.P., Ffowcs Williams, J.E., Heckl, M., Leppington, F.G., Modern Method in analytical Acoustics-Lecture Notes, Spinger-verlag, 1992

[5] di Francescantonio P. A New Boundary Integral Formulation for the Prediction of Sound Radiation[J], Journal of Sound and Vibration, 1997, 202(4):191～509.

[6] Brentner, K.S., Modeling Aerodynamically Generated Sound: Recent Advance in Rotor Noise Prediction, AIAA Paper, 2000-0345, 2000.

[7] Han Z.H., Song W.P., Qiao Z.D., Investigation of Rotor Noise Prediction Using Different Aeroacoustic Methods in Time Domain, 24th International Congress of the Aeronautical Sciences, ICAS 2004-3.4.R, Yokohama, Japan, 2004.

[8] Rizzi, A., Eriksson, L.E., Transfinite Mesh Generation and Damped Euler Equation Algorithm for transonic Flow Around Wing-Body Configuration.. AIAA Paper 81-0999, 1981.

[9] Qiao, Z.D., Yang A.M. and Zhu.B. Computation of The Unsteady Viscous Flow About Helicopter Rotors In Forward Flight By A Full Implicit Dual Time Method, AIAA 03-408221st AIAA Applied Aerodynamic Conference June 23-26, 2003.

[10] Jameson A, Schmidt W, Turkel E. Numerical Solutions of the Euler Equations by a Finite Volume Method using Runge-Kutta Time Stepping Schemes. AIAA Paper 81-1259, 1981.

[11] Lin, C.Q., Pahlke, K., Numerical Solution of Euler Equations for Aerofoil in Arbitrary Motion, Aeronautical Journal, June/July, 1994, pp.207-214

[12] Caradonna F.X., Tung, C., Experimental and Analytical Studies of a Model Helicopter Rotor in Hover, NASA Technical Memorandum 81232, National Aeronautics and Space Administration, 1981.

[13] Boxwell, D.A., Yu, Y.H. and Schmitz, F.H., Hovering Impulsive Noise: Some Measured and Calculated Results. Vertica, Vol.3, pp.35-45, 1979.

[14] Kuntz M. Rotor Noise Prediction in Hover and Forward Flight Using Different Aeroacoustic Methods[R], AIAA Paper 96-1695